Proceedings of the ASME 2010 3rd Joint US-European Fluids Engineering Summer Meeting and 8th International Conference on Nanochannels, Microchannels, and Minichannels
FEDSM-ICNMM2010
August 1-5, 2010, Montreal, Canada

FEDSM-ICNMM2010-30725

NUMERICAL INVESTIGATIONS OF ACTIVE FLOW CONTROL USING SYNTHETIC JETS ON A HIGHLY LOADED COMPRESSOR STATOR CASCADE

Christoph Gmelin[*], **Mathias Steger**, **Vincent Zander**, **Wolfgang Nitsche**, **Frank Thiele**
Technische Universität Berlin
Strasse des 17. Juni 135
10623 Berlin, Germany
Email: christoph.gmelin@cfd.tu-berlin.de

André Huppertz, **Marius Swoboda**
Rolls-Royce Deutschland Ltd. & Co. KG
Eschenweg 11, Dahlewitz
15827 Blankenfelde-Mahlow, Germany
Email: andre.huppertz@rolls-royce.com

ABSTRACT

Time-resolved Reynolds-Averaged Navier-Stokes simulations of a 3D stator compressor cascade are performed. At the design point of the airfoil under investigation, pronounced secondary flow effects are observed. Strong corner vortices emerge from the casing walls and the flow separates from the blade suction side towards the trailing edge. Transition from laminar to turbulent flow occurs within a laminar separation bubble. Using a commercial CFD software, the influence of the spatial resolution is investigated by means of a spanwise coarsening and refinement of the created mesh. Zero net mass flux synthetic jet actuation is used to control the separated regions. The work presents a variation of the temporal discretization and an analysis of the driving parameters of the actuation.

NOMENCLATURE

Geometric and Flow Quantities

$c_p = {}^{(p-p_1)}/_{q_1}$	1	pressure coefficient
c_μ	1	momentum coefficient
h	m	blade height
l	m	chord length
l_a, w_a, d_a	m	actuator length, width, depth
Ma	1	Mach number
p_t	Pa	total pressure
p	Pa	static pressure
$q = {}^{\rho}/_{2} \cdot V^2$	Pa	dynamic pressure
Re	1	Reynolds number
s	m	length from leading edge
S	m	total length of suction side
$St = {}^{f \cdot l}/_{V_1}$	1	Strouhal number
T_t	K	total temperature
t	m	pitch
V	${}^{m}/_{s}$	velocity
$\hat{V}$	${}^{m}/_{s}$	peak velocity
$\overline{V}$	${}^{m}/_{s}$	mean velocity
W_F	W	mean fluid power
x, y, z	m	coordinate system
y^+	1	dimensionless wall distance
α	deg	flow angles
γ	deg	stagger angle
$\zeta_V = {}^{(p_{t,1}-p_{t,2})}/_{q_1}$	1	total pressure loss
${}^{\Delta p}/_{q_1} = {}^{(p_2-p_1)}/_{q_1}$	1	pressure rise
κ	1	adiabatic exponent
μ	Pa s	dynamic molecular viscosity
ν	${}^{m^2}/_{s}$	kinematic viscosity
ν_t	${}^{m^2}/_{s}$	turbulent kinematic viscosity
ρ	${}^{kg}/_{m^3}$	density
τ_w	Pa	wall shear stress
φ	deg	injection angle

[*]Address all correspondence to this author.

Subscripts

AFC	actively controlled flow
base	base flow
b	blade
c	casing
exp	experiment
sim	simulation
x, y, z	component in x,y,z direction
1	inlet
2	outlet

INTRODUCTION

By increasing the maximum load per compressor stage, more compact jet engines could be built, with reduced weight and thus greater efficiency [1]. In today's gas turbine engines, the stage load is particularily maxed out by passive flow control methods such as blade sweep [2], three–dimensional airfoil designs [3], and vortex generators at the side walls [4]. Still, for safety and reliability reasons, the engines have to run far away from their optimal operating point in order to prevent instabilities like stall and surge whose consequences can impair or even destroy the whole engine [5]. Recently, *Active* Flow Control (AFC) methods are considered in order to extend the working range of jet engines. Within the scope of turbomachinery application, Lord et al. [6] give an overview of possible flow control opportunities in gas turbine engines.

Computational Fluid Dynamics (CFD) by means of Reynolds-Averaged Navier-Stokes (RANS) simulations has become a helpful tool within the industrial design process of turbomachinery blades. Thus, an important first step for the interpretation of active flow control concepts is the determination of the feasibility to predict the impact of AFC within an industrial numerical approach. Considering unsteady blowing or suction at casing endwalls or blade surfaces, the main question consists in the reliability of the results from a simulation which does not comprise all details of the complex flow phenomena involved in active flow control via jets. Therefore, the attention is turned to the feasibility of predicting correct trends with respect to the characteristic flow control parameters.

The work presented considers active flow control by means of zero net mass flux Synthetic Jet (SJ) actuation at a linear compressor stator cascade. The investigated Controlled Diffusion Airfoil (CDA) has a highly loaded design point and represents the possible blading of next generation jet engines. Due to its low aspect ratio and the strong flow turning, pronounced secondary flow structures arise, representing a challenge for RANS simulations with respect to the turbulence modeling. Especially the grid resolution in spanwise direction is found to be decisive for the quality of the simulation results. Additionally, laminar flow separation with subsequent transition from laminar to turbulent flow over a laminar separation bubble and fully turbulent reattachment is observed, which has to be respected within the simualtion as well.

The industrial approach is realized within the commercially available finite-volume Navier-Stokes solver $FINE^{TM}/Turbo\ v.8.6-1$ [7] from *NUMECA International*, specialized for turbomachinery application. The one-equation turbulence model of Spalart-Allmaras (SA model) [8] is used in combination with fixed transition on the blade surfaces. The base flow is analyzed in detail on three grids with different spatial resolution in spanwise direction. Evaluation with the help of experimental data enforces the necessity of the chosen resolution and shows that the improvement of the results by further refinement is not worth the additional numerical costs.

Zero net mass flux synthetic jet excitation is applied in order to control the secondary flow. The main advantage of SJ actuation is that there is no need for additional fluid supply accompanied by piping and compressors necessary for steady jets. A SJ is formed directly from the working fluid of the flow system in which it is deployed. On top, active flow control is often more efficient if the energy input and the injected momentum are diminished [9]. General aspects of CFD, such as grid resolution, time discretization, and turbulence modeling with respect to SJ simulation have been investigated within the workshop "CFD Validation of Synthetic Jets and Turbulent Separation Control" in 2004 [10]. Even though it mainly concludes that state-of-the-art CFD methods, especially URANS, are not fully adequate to accurately predict the unsteady flow of synthetic jets, the influence of the temporal discretization of the actuation is analyzed. The time steps per period of the actuation and the internal iterations per time step are varied within the order of magnitude practicable for industrial application and the impact on the simulation results is investigated.

The influence of the injected mass during the blowing phase of the jet and the jet velocity amplitude ratio are investigated by means of a variation of the actuator width and consequently the slot area and a variation of the jet velocity amplitude. The resulting effects on the efficiency of the cascade are related to the momentum coefficient c_μ, which is proportional to the slot width and the square of the mean jet velocity, and the power of the added fluid W_F, proportional to the slot width and the cube of the mean jet velocity. Thus, the parameter which the global effects are related to is decisive for judging the benefit of the actuation.

Previously performed work on the same stator cascade configuration include analyses on the effects of transition modeling [11], an extensive parameter variation of synthetic jet actuation at two different control locations [12], and investigations on pulsed excitation at the casing endwalls [13] where results in good agreement to the accompanying experiments [14] could be produced using the same industrial approach with similar numerical methods.

TABLE 1. GEOMETRICAL PARAMETERS OF THE STATOR CASCADE.

Parameter	Variable	Value	Unit
Chord length	l	0.375	m
Suction side length	S	0.42	m
Aspect ratio	h/l	0.8	1
Pitch to chord ratio	t/l	0.4	1
Stagger angle	γ	20	deg
Inflow angle	α_1	60	deg
Outflow angle	α_2	0	deg

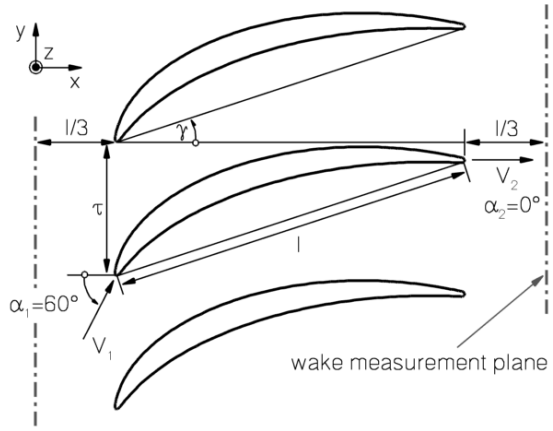

FIGURE 1. GEOMETRY OF THE STATOR CASCADE WITH INLET AND OUTLET EVALUATION PLANE.

CASCADE AERODYNAMICS

The stator cascade consists of Controlled Diffusion Airfoils (CDA) with a chord length of $l = 0.375$m. At the investigated design point, the incoming flow has a velocity of $V_1 = 34 m/s$ at an inflow angle of $\alpha_1 = 60°$. With a constant total temperature of $T_{t,1} = 294$K at the inlet, the corresponding chord Reynolds number is $Re_l = 840,000$ and the resulting inflow Mach number is $Ma_1 = 0.1$. Due to the relatively small pitch to chord ratio of $t/l = 0.4$, the high turning angle of up to $\Delta\alpha = 60°$, and the low aspect ratio of $h/l = 0.8$, the airfoil is designed to be highly loaded and therefore strong secondary flow structures can be expected. The geometrical parameters are summarized in Tab. 1, and an overview of the stator cascade is shown in Fig. 1.

Autonomous experiments are carried out on a low speed cascade test section at the Department of Aeronautics and Astronautics of the Berlin Institute of Technology by Zander [15] and Hecklau [16, 17].

TABLE 2. BOUNDARY CONDITIONS.

Inlet	Inflow angle	α_1	60	deg
	Total temp.	$T_{t,1}$	293.95	K
	Total pressure	$p_{t,1}(z)$	-	Pa
	Turb. viscosity	$\nu_{t,1}$	$7.154 \cdot 10^{-5}$	m^2/s
Outlet	Static pressure	p_2	102417	Pa

COMPUTATIONAL METHOD

Within the frame of the presented computations, the commercial CFD software package $FINE^{TM}/Turbo$ *v*.8.6 − 1 [7] from *NUMECA Int.* has been employed. Since the appendant grid generator for turbomachinery (*AutoGrid* [18]) only offers limited meshing opportunities for linear cascades, grids are created with *G3DMESH* [19], a tool developed at DLR Cologne. Grid pre-processing as well as local refinements and modifications for actuator nozzle attachments are realized within *IGG* [20], a structured grid generator from *NUMECA Int.*.

The flow solver *EURANUS* solves the 3D Reynolds-Averaged Navier-Stokes equations on general structured non-orthogonal multi-block grids. The flexibility of the structured grids is greatly enhanced by use of so-called "Full Non-Matching Connections", a technique which allows arbitrarily connecting grid blocks of different grid topologies or point numbers to each other without numerical interpolation losses.

The numerical algorithm incorporated into *EURANUS* is an explicit four stage Runge-Kutta scheme [21]. A variety of convergence acceleration techniques are employed, such as implicit residual smoothing [22], dual time stepping [23], and a full multigrid algorithm, which is used in a W-cycle on three full multigrid levels. Space integration is performed using a second order cell-centred finite volume discretization with fourth order artificial dissipation.

In the scope of the present work, the one-equation model of Spalart and Almaras [8] is used in combination with fixed transition on the blade surfaces. This is realized by taking the influence of an intermittency parameter into account, which triggers the production term of the turbulence model. The intermittency is zero within the laminar and one within the turbulent flow regime.

The boundary conditions for all calculations are listed in Tab. 2. The boundary layer of the incoming flow is accounted for by imposing a spanwise profile of the total pressure $p_{t,1}(z)$, measured at a plane corresponding to the inlet of the computational domain. The desired inlet flow Mach number $Ma_1 = 0.1$ is achieved by variation of the constant static pressure p_2 imposed at the outlet boundary located 2.4 times the chord length downstream of the blade trailing edge.

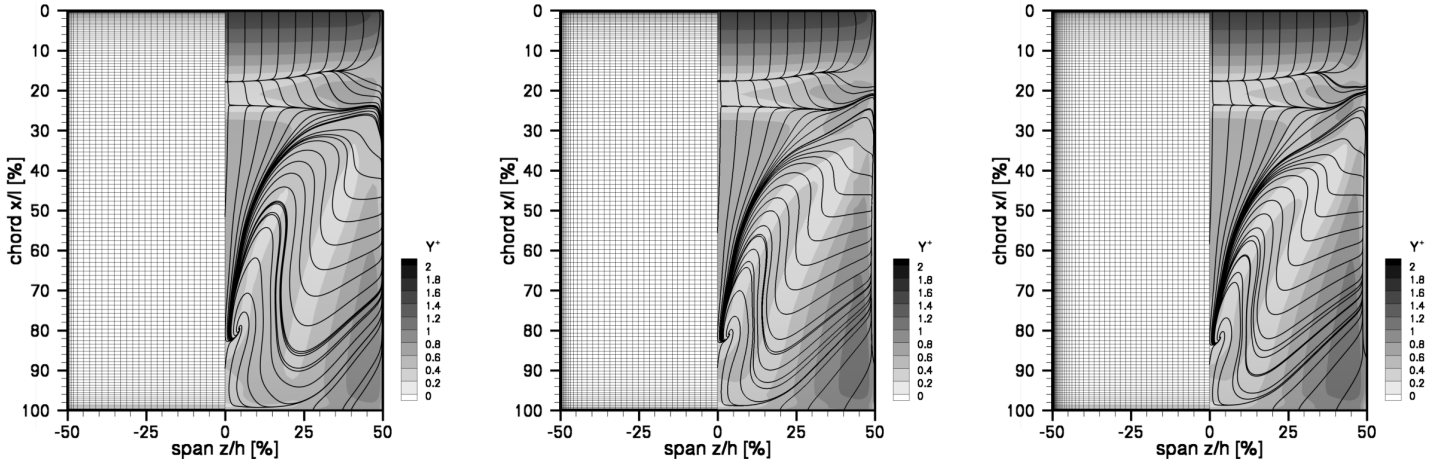

(a) COARSE GRID. (b) BASE GRID. (c) FINE GRID.

FIGURE 2. SPANWISE GRID RESOLUTION OF THE THREE INVESTIGATED GRIDS AND RESULTING DISTRIBUTION OF THE DIMENSIONLESS WALL DISTANCE y^+ OVERLAID WITH WALL STREAMLINES DEFINED BY WALL SHEAR STRESSES - FLOW DIRECTION FROM TOP TO BOTTOM.

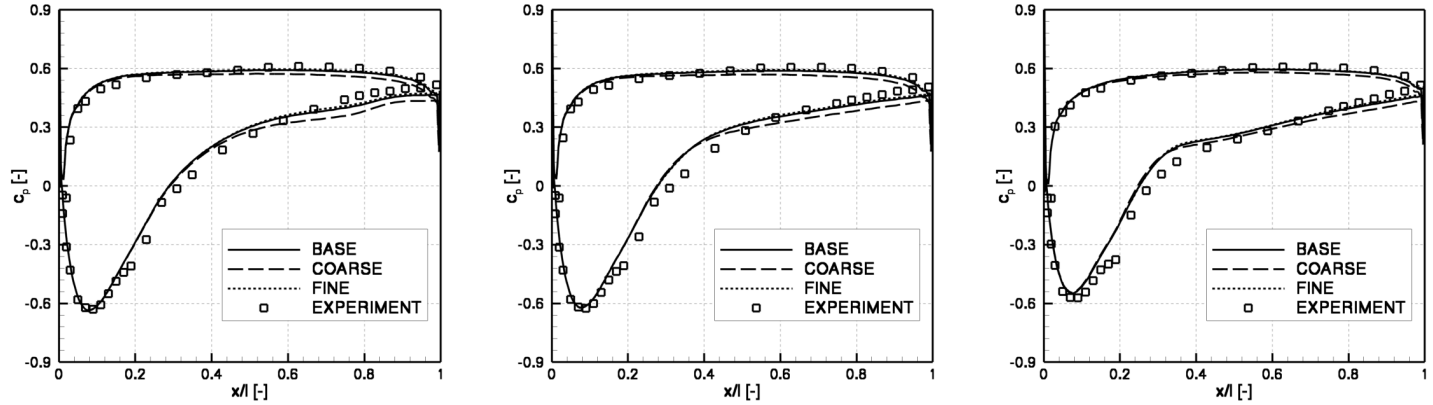

(a) 0% SPAN (MIDSPAN). (b) 20% SPAN. (c) 40 % SPAN (CASING).

FIGURE 3. PRESSURE COEFFICIENT DISTRIBUTION FOR THE THREE INVESTGATED GRIDS AT THREE SPANWISE POSITIONS WITH COMPARISON TO EXPERIMENTAL DATA [15].

SPANWISE GRID RESOLUTION

The primarily created "base grid" is coarsened and refined in the direction of the blade height by increasing and decreasing the number of grid points by 25%, respectively. Within the base grid, the spanwise direction is resolved by 97 points. Overall, approximately two million grid cells are used. Coarsening the grid in the direction of the blade height by 25% results in a "coarse grid" with approximately 1.5 million grid cells where the span is resolved by 73 points. The "fine grid" uses 2.5 million grid cells in total and 121 points along the span. All three grids provide the same grid size for the first grid cell at the casing endwalls and all grid cells have an aspect ratio below 1424 and an expansion ratio below two.

The resulting grid cell distribution is depicted in Fig 2 over the half span of the blade suction side for the three grids investigated. The other half of each span shows the distribution of the dimensionless wall distance y^+, overlaid with numerically calculated wall streamlines defined by the vector of the wall shear stress $\tau_{w,xyz}$ at the first grid cell next to the wall. Flow direction is from the top to the bottom of the figure. The maximum dimensionless wall distance is $y^+{}_{max} < 2$ for all grids. The wall streamlines on the blade suction side illustrate the secondary flow developing in the cascade. In general, the laminar boundary layer separates towards the rear of the blade suction side surface, forming a laminar separation bubble. The separated flow undergoes transition, reattaching on the blade suction surface as a turbu-

TABLE 3. INTEGRAL AVERAGED VALUES FOR BASE FLOW COMPUTATIONS AND EXPERIMENT.

	COARSE	BASE	FINE	EXPERIMENT
ζ_V	0.117	0.107	0.105	0.106
$\Delta p/q_1$	0.541	0.555	0.558	0.565

lent boundary layer. At the streamwise position of the turbulent reattachment, secondary flows caused by the endwalls come into effect. The main flow is narrowed in the streamwise direction. Between the secondary and the main flow, a 3D separation line is formed, ending up at midspan, where separation nearly perpendicular to the principal flow occurs.

The simulation captures the general secondary flow pattern on all three grids. Distinct discrepancies can be found on the coarse grid (Fig. 2(a) at the positon of the turbulent reattachment next to the casing endwall, where the secondary flow from the endwalls comes into effect. Compared to the base and the fine grid (Fig. 2(b), 2(c)), the size of the laminar separation bubble is overpedicted and the penetration of the main flow by the secondary flow is stronger. Refinement of the base grid results in no visible change of the secondary flow pattern.

Further insight into the grid dependency is achieved in Fig. 3, showing the pressure coefficient distribution c_p at three spanwise positions for the three investigated grids in comparison to experimental data [15]. Over the whole span, the simulation on the coarse grid (long dashed line) underpredicts the pressure downstream of 20% chord length on the pressure side and 35% chord on the suction side by approximately 5 - 10% compared to the simulation on the base grid (solid line). The simulation on the fine grid (short dashed line) shows the same distribution over the whole span as the computation on the base grid. Compared to the experimental data, the base grid solution predicts the pressure peak well along the span with small discrepancies at 40% span. At midspan, the agreement is equally good for pressure and suction side. Downstream of 70% chord the pressure is slightly underpredicted by the simulation. At 20% span, discrepancies can be found at around 40% chord length, where the simulation overpredicts the pressure. Close to the casing, at 40% span, the pressure is overestimated at the suction side until 45% chord length. Further downstream the agreement of simulation and experiment is pretty good.

Since the global efficiency of the stator cascade is determined by the total pressure loss and the pressure rise, the prediction of these values is of high interest. The total pressure loss is herein mass-averaged, whereas the pressure rise is area-averaged at evaluation planes one third of the chord length upstream of the leading edge and one third of the chord length downstream of the trailing edge (cf. Fig. 1).

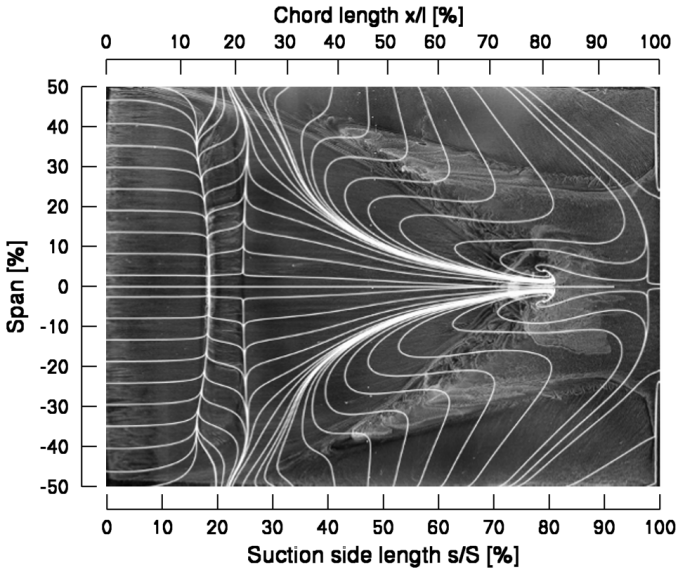

FIGURE 4. SIMULATED WALL STREAMLINES ON BASE GRID ABOVE OIL FLOW VISUALIZATION OF THE EXPERIMENT [15].

The integral averaged values of the base flow simulations on the three grids are listed and compared to experimental data in Tab. 3. All simulations underpredict the pressure rise, but the difference decreases with increassing spanwise resolution. The discrepancy for the coarse grid is moer than 4%. For the base grid the error is reduced to 1.8%, whilst it is still 1.2% for the fine grid. The total pressure loss is massively overpredicted by the coarse grid solution, with an error of over 10% with respect to the experimental data. The base grid on the other hand predicts the losses very well with an error below 1%. This accuracy can not be improved by further grid refinement.

The results presented show the necessity to spatially resolve the span at least with the number of grid points from the "base grid", i.e. 97 points. Further refinement shows that the spatial resolution reaches kind of a saturation at this point. The additional grid points of the "fine grid" do not improve the results in a manner that would justify the increased computational costs.

The existent discrepancies between simulation and experiment are ascribed to a general ovepreddiction of the secondary flow as shown in Fig. 4, comparing the numerical wall streamlines of the basic grid simulation to an underlying oil flow visualization of the experiment [15]. The discrepancy of the shape of the intersection line between secondary flow emerging from the endwalls and main flow, as well as the resultant slightly downstream delayed separation at midspan give explanation for the differences in the pressure coefficient distribution and the integral average value of the pressure rise. These facts are extensively discussed in [12]. Here, the attention was turned to the influence of the grid resolution in spanwise direction.

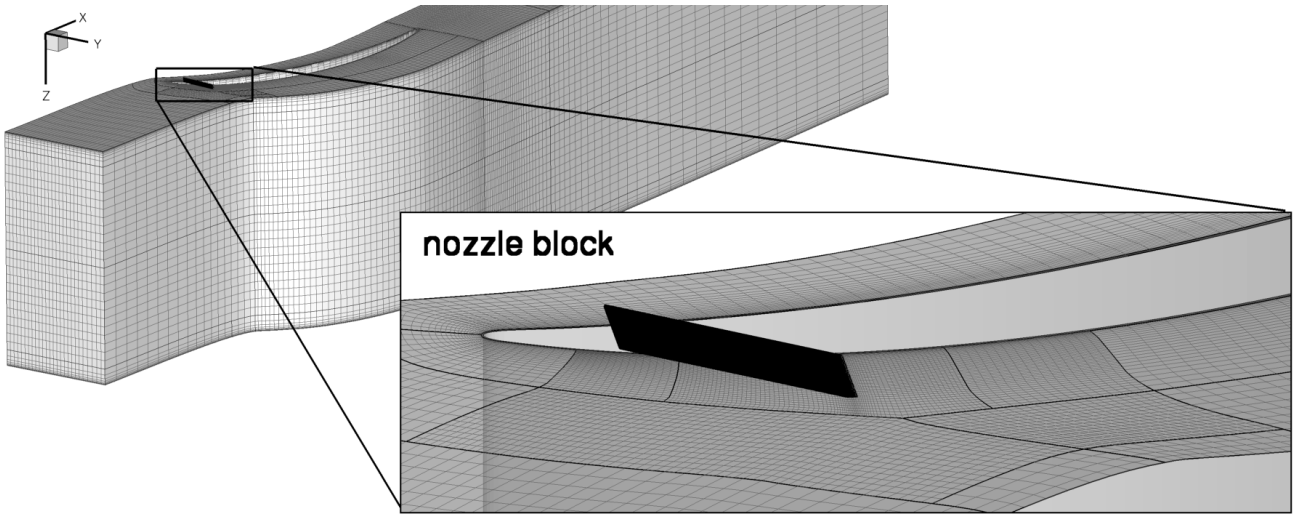

FIGURE 5. OVERVIEW OF THE COMPUTATIONAL DOMAIN SHOWING EVERY SECOND GRID CELL AND DETAIL VIEW OF THE REFINEMENT FOR THE ACTUATION AT THE CASING WITH ATTACHED NOZZLE ACTUATOR BLOCK.

SPATIAL AND TEMPORAL DISCRETIZATION OF THE SYNTHETIC JET ACTUATION

Due to the time scale of the unsteady SJ phenomena being of the same order of magnitude as the turbulent time scale, URANS models fail in the prediction of the complex flow structures involved with synthetic jets. The industrial approch performed in this work does not claim to resolve the synthetic jet actuation itself, nor the complex flow phenomena involved in greater detail. Still, to not enforce the dissipative character of the URANS simulation, the grid is refined at the vicinity of the actuation and the temporal resolution of the excitation is varied within a range practicable for industrial application.

The synthetic jet actuation is realized via nozzle blocks which spatially resolve the actuators at the casing endwalls. A neat momentum transfer is guaranteed by resolving the actuator slot within the main computational domain. Therefore, the grid is refined locally at the vicinity of the actuation with the help of non-matching connections as shown in Fig. 5. Thus, the number of grid cells increases to 2.5 million and an acceptable mean of spatial resolution and computational effort is granted.

Time-resolved RANS simulations are, even nowadays, rarely used within the industrial design process. This is due to the exploding computational cost if transient effects are respected. More challenging than the spatial discretization is therefore the temporal resolution of the sinusoidal excitation signal applied at the free face of the nozzle actuator block. The CFD workshop on SJ validation [10] showed that even 1000 time steps per excitation phase may not be sufficient to capture all the unsteady flow phenomena. This is out of range for industrial CFD (and probably will be for a while) and therefore not considered here. The question in this work is, how the effect of synthetic jet actuation on the global efficiency is influenced by the temporal resolution of an industrial approach.

In previous simulations (cf. [12]) an extensive variation of the parameters involved in synthetic jet actuation was performed. Thereby, one phase of the actuation was resolved by 20 time steps and 30 internal iterations (ii) were performed for each time step (step). Here, the number of time steps per phase or the internal iterations per time step are increased and decreased for one parameter set. The effect on the global efficiency is considered by means of total pressure loss and pressure rise or the reduction and gain of these values with respect to the base flow.

Five temporal discretizations are investigated. With respect to the previously used setup with 20 time steps per phase and 30 internal iterations per time step, a finer resolution with 40 time steps, and a coarser one with only 12 time steps per phase are considered, without changing the number of internal iterations. Further, the number of internal iterations is varied whilst the number of time steps per phase is kept constant at a value of 20. With respect to the standard discretization, the number of internal iterations are nearly doubled to 50 and reduced to 20.

As the spatial resolution is related to the phase of the excitation, the resulting excitation signal is analyzed first. Therefore, the jet velocity ratio v_{jet}/v_1 at the nozzle actuator slot is shown over the time, in Fig. 6(a) for the variation of the number of time steps per phase, and in Fig. 6(b) for the variation of the internal iterations per time step. A similar excitation signal is predicted by all temporal discretizations investigated. Especially the peak velocity ratios at blowing and suction phase agree. Nameable differences can only be found for the two coarser resolutions during rising velocity at both blowing and suction phase. The discrepancies are more distinct for the low number of internal iterations.

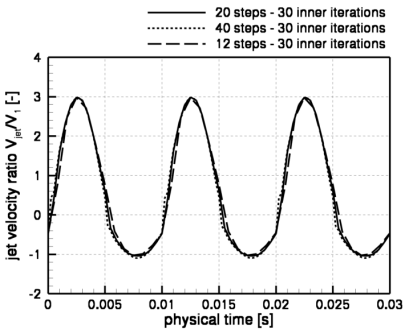

(a) VARIATION OF THE NUMBER OF TIME STEPS PER PHASE OF THE EXCITATION SIGNAL.

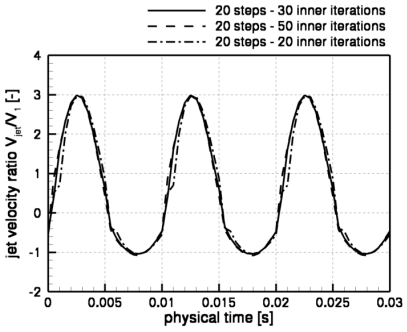

(b) VARIATION OF THE INNER ITERATIONS PERFORMED PER TIME STEP.

FIGURE 6. JET VELOCITY RATIO OVER TIME FOR VARYING TEMPORAL DISCRETIZATIONS.

It is assumed that at least 30 internal iterations should be accomplished for each time step. This value represents the standard of the flow solver.

The resulting effects on the global efficiency are summarized in Tab.4 for the five cases investigated. If the number of time steps per phase is doubled to 40, the total pressure loss is predicted unchanged down to the third position after the decimal point. Still, the reduction, rounded to half of a percent, is lower by one percentage point. A higher value for the pressure rise is predicted and the gain differs by one percent as well. If the resolution is decreased to 12 time steps per phase, lower values are predicted for the total pressure loss and the pressure rise. The difference of the reduction and the gain to the reference case with 20 time steps per phase lie at 1% and 0.5% respectively.

Variation of the number of internal iterations per time step results in equivalent trends. For an increased number of iterations, i.e. here 50, the value of the total pressure loss remains unchanged until the third decimal place but the pressure rise increases. A decrease of the internal iterations to 20 results in a lower value of the total pressure loss and therfore an increased reduction with respect to the base flow. The value of pressure rise is smaller as well.

TABLE 4. INTEGRAL AVERAGED VALUES FOR VARYING TEMPORAL DISCRETIZATIONS.

	ζ_V	reduction	$\Delta p/q_1$	gain
20 steps, 30ii	0.098	9%	0.577	4%
40 steps, 30ii	0.098	8%	0.581	5%
12 steps, 30ii	0.097	10%	0.574	3.5%
20 steps, 50ii	0.098	8.5%	0.579	4.5%
20 steps, 20ii	0.097	9.5%	0.576	4%

It can be seen, that variation of the temporal discretization has only a small effect on the global outcome of the actuation, at least within the range investigated. With the chosen resolution of 20 time steps per phase and 30 internal iterations per time step, each unsteady simulation takes approximately five days on 16 CPUs with 2.4GHz. The simulation time is directly proprtional to the number of time steps times the internal iterations performed, and the cost of the computation is directly proprtional to the simulation time. It is therefore unpracticable to increase the temporal discretization within the industrial approach pursued.

INVESTIGATIONS ON THE MASS FLOW RATE AND THE JET VELOCITY OF THE SYNTHETIC JET

A synthetic jet actuation can be characterized by three parameters: the jet velocity amplitude ratio $\hat{v}_{jet}/v_1$, the excitation frequency f represented by the Strouhal number $St = f \cdot l/v_1$, and the injection angle φ between the wall and the jet. These parameters have been thoroughly investigated in previous works [12].

The actuator used in these previous investigations has a width of $w_a = 0.4$mm. By variation of the jet velocity amplitude ratio $\hat{v}_{jet}/v_1$ it could be shown that the impact of the actuation mainly depends on the strength of the jet. If the oscillatory jet momentum is considered instead of the jet velocity ratio, by means of the momentum coefficient c_μ, it becomes obvious that the momentum of the excitation can be increased by enlarging the actuator slot and thus increasing the mass flow rate of the excitation. Another approach considers the mean fluid power of the excitation W_F which is directly proportional to the electrical power required for the actuation and therefore a useful parameter in order to determine the overall efficiency of the control concept with respect to the effeciency gain of the compressor cascade achieved by the synthetic jet actuation. The main difference of these two parameters is the impact of the jet velocity amplitude $\hat{V}_{jet}$, which is respected by the power of two by the momentum coefficient c_μ and by the power of three by the mean fluid power W_F, whilst both parameters are directly proportional to the width of the actuator slot w_a.

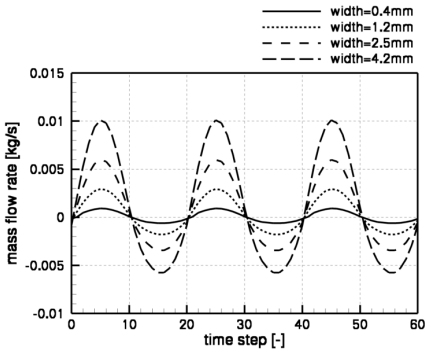

(a) VARIATION OF THE MASS FLOW RATE AT ACTUATOR SLOT.

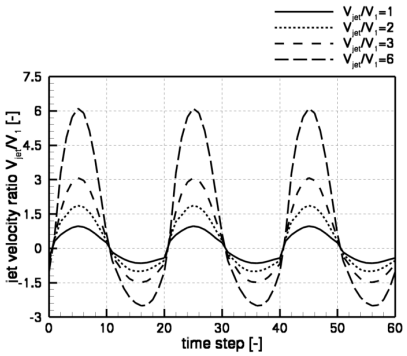

(b) VARIATION OF THE JET VELOCITY RATIO AT ACTUATOR SLOT.

FIGURE 7. DIFFERENT JET VELOCITY AMPLITUDE RATIOS AND MASS FLOW RATES OF THE SYNTHETIC JET ACTUATION.

In this work the momentum coefficient according to Greenblatt [9] is used, defined as:

$$c_\mu = \frac{\rho_{jet} \cdot \overline{V}_{jet}^2 \cdot w_a}{l \cdot \rho_1/2 \cdot V_1^2} \tag{1}$$

The mean fluid power is defined as proposed by Crowther and Gomes [24]:

$$W_F = \frac{1}{2} \rho_{jet} w_a l_a \overline{V}_{jet}^3 \tag{2}$$

For a sinusoidal varying excitation signal the mean jet velocity is $\overline{V}_{jet} \approx \frac{1}{3} \cdot \hat{V}_{jet}$.

The impact of the mass flow rate of the excitation is investigated and compared to the previously performed variation of the jet velocity ratio by means of a variation of the actuator width w_a. Therefore, three additional actuators with varying actuator width, i.e. $w_a = 1.2$mm, $w_a = 2.5$mm, and $w_a = 4.2$mm are considered.

Simulations are performed with synthetic jets applied at the four actuators. The jet velocity amplitude ratio is ${}^{V_{jet}}/_{V_1} \approx 3$ and the excitation frequency corresponds to a Strouhal number of $St \approx 1$. The resulting mass flow rate at the slot of the actuator is depicted in Fig. 7(a) for the four computations. The desired increase of the mass flow rate by the enlarged actuator width is clearly visible. Fig.7(b) shows the jet velocity ratio with respect to the inflow velocity of the cascade for the four comparative simulations on the actuator with a width of $w_a = 0.4$mm. The jet velocity amplitude is varied from ${}^{V_{jet}}/_{V_1} \approx 1$ to ${}^{V_{jet}}/_{V_1} \approx 6$. As both plots show the values at the slot of the actuator, where the jet enters the main domain of the cascade, the jet velocity, and thus the mass flow rate, are higher during the blowing phase than during the suction phase. At the free face of the actuator, where the sinusoidal boundary condition is applied, this velocity or mass deficit does not exist. Measurements of a synthetic jet in quiescent air, performed by the experimental partner, show a similar distribution of the jet velocity next to the actuator slot with satisfying aggreement to the simulation as shown in [12]. Thus, the decision of spatially discretizing the actuator by a simple nozzle block proves to be right.

The results of the mass flow rate and the jet velocity amplitude variation are shown in Fig. 8 by means of the percentage change of the integral averaged values of total pressure loss and pressure rise with respect to the uncontrolled base flow over the momentum coefficient c_μ and the mean fluid power W_F. The solid line represents the variation of the mass flow rate on different actuator widths and the dashed line illustrates various jet velocity amplitudes investigated on the original actuator. The general impact of the actuation shall be discussed first. For jet velocity amplitude ratios above one, the total pressure loss is reduced (negative percentage values) and the pressure rise is increased (positive percentage values). The achieved reduction or gain increases for rising jet velocity amplitudes as well as for rising mass flow rates. Thereby, no saturation could be observed within the investigated range.

The effects are first related to the momentum coefficient c_μ in Fig. 8(a) and Fig. 8(b). Regarding the reduction of the total pressure loss (Fig. 8(a)), an increase of the jet velocity amplitude is more efficient than enlarging the actuator slot. With the smallest actuator, a reduction of -12% can be reached for a momentum coefficient below $4 \cdot 10^{-3}$. In order to achieve the same reduction by enlarging the slot, a value close to $c_\mu = 6 \cdot 10^{-3}$ is necessary. The gain of pressure rise on the other hand is slightly greater for an increased mass flow rate than for the higher jet amplitude with the equivalent momentum coefficient.

A slightly different trend is observed if the effects are related to the mean fluid power W_F, as shown in Fig. 8(c) and Fig. 8(d). As the mean fluid power respects the jet velocity by the power of three, excitation with an increased mass flow rate is mostly more beneficial. Only for a very small range the total pressure loss is further reduced with less effort by rising the jet veloc-

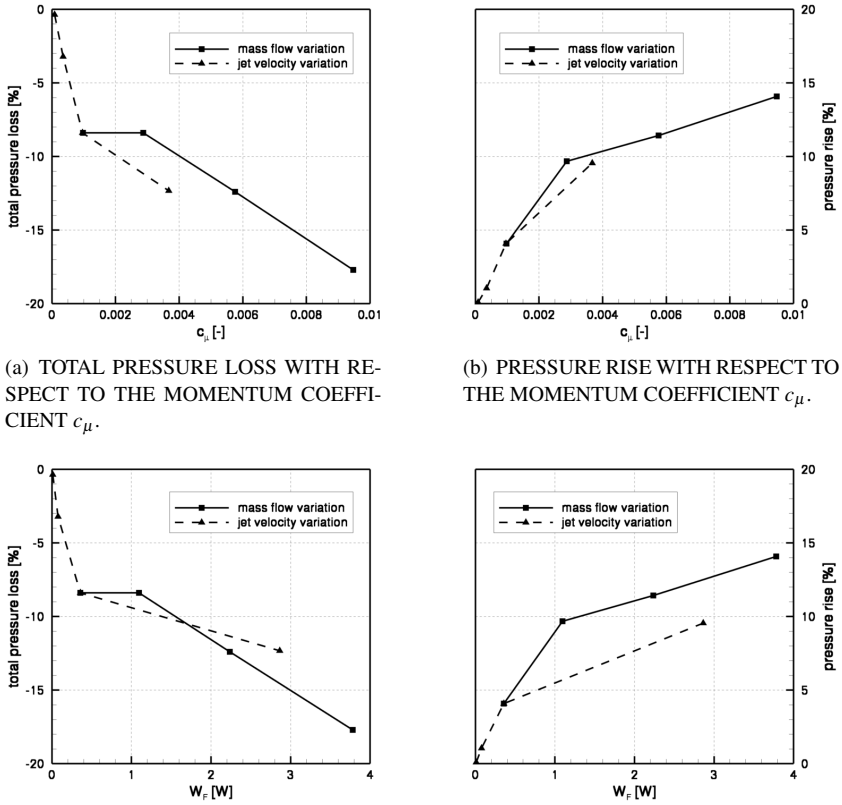

(a) TOTAL PRESSURE LOSS WITH RESPECT TO THE MOMENTUM COEFFICIENT c_μ.

(b) PRESSURE RISE WITH RESPECT TO THE MOMENTUM COEFFICIENT c_μ.

(c) TOTAL PRESSURE LOSS WITH RESPECT TO THE MEAN FLUID POWER W_F OF THE JET.

(d) PRESSURE RISE WITH RESPECT TO THE MEAN FLUID POWER W_F OF THE JET.

FIGURE 8. EFFECT ON THE GLOBAL EFFICIENCY OF THE CASCADE BY MEANS OF TOTAL PRESSURE LOSS AND PRESSURE RISE FOR VARIATION OF THE JET VELOCITY RATIO AND THE MASS FLOW RATE OF THE SYNTHETIC JET ACTUATION.

ity instead of increasing the mass flow rate. The benefit of the enlarged slot is clearly visible regarding the gain of pressure rise (Fig. 8(d)) with respect to the mean fluid power. Within the range covered by both approaches, the gain increases nearly constant by approximately 50% for the equivalent fluid power achieved by either variation of the jet velocity ratio or the mass flow rate.

It is important to state that beneficial effects could only be observed for jet velocity amplitude ratios above one. Even though variation of the mass flow rate is only performed for one constant jet velocity ratio it seems plausible that increasing the mass flow rate is the appropriate way to increase the effects and simultaneously diminish the effort, since the energetical power is directly proportional to the mean fluid power which respects the jet velocity by the power of three.

CONCLUSION

Time-resolved Reynolds-Averaged Navier-Stokes simulations of a highly loaded 3D linear compressor cascade were performed. Hereby, an industrial approach is pursued by means of computational effort and costs, as well as the commercial software package employed. Analyses of the base flow revealed strong secondary flow structures. The results proved to be sensitive towards the spatial resolution in spanwise direction. Investigations on a coarser and a finer grid resolution along the span showed nearly saturated results on the chosen grid with good agreement to experimental data.

Active flow control by means of synthetic jets is applied at the casing endwalls of the stator cascade. The influence of the temporal discretization with respect to the excitation signal is investigated within the limits of an industrial application. Increasing the number of time steps or the internal iterations per phase of the excitation by a factor of two turned out to not improve the results in an order that would justify the according rise of the computational costs.

Separate variation of the mass flow rate and the jet velocity ratio of the synthetic jet are considered with respect to the global effects on the efficiency of the cascade. The effort involved in the actuation is related to the momentum coefficient c_μ and the mean

fluid power W_F, respectively. It can be shown that for a given jet velocity ratio, the increase of the mass flow rate by enlarging the actuator width becomes more efficient than a further increase of the jet velocity itself.

ACKNOWLEDGMENT

The work presented in this paper is performed in close cooperation with Rolls-Royce Deutschland Ltd. & Co. KG as part of the European Union founded research project TATMo - Turbulence and Transition Modeling for Special Turbomachinery Applications, FP6-2005-AERO-1-030939. The authors would like to thank for the support of the work and the permission to publish.

REFERENCES

[1] Wennerstrom, A.J., 1990. "Highly Loaded Axial Flow Compressors: History and Current Developments". *ASME Journal of Turbomachinery,* ***112***, pp. 567–578.

[2] Gallimore, S.J., Bolger, J.J., Cumpsty, N.A., Taylor, M.J., Wright, P.I., and Place, J.M.M., 2002. "The Use of Sweep and Dihedral in Multistage Axial Flow Compressor Blading–Part I and II". *ASME Journal of Turbomachinery,* ***124***, pp. 521–542.

[3] Staubach, J.B., Sharma, O.P., and Stetson, G.M., 1996. "Reduction of Tip Clearance Losses Through 3-D Airfoil Designs". *IGTI 96-TA-013*.

[4] Hergt, A., Meyer, R., and Engel, K., 2006. "Experimental Investigation of Flow Control in Compressor Cascades". *ASME GT2006-90415*.

[5] Bräunling, W.J.G., 2009. *Flugzeugtriebwerke*. Springer.

[6] Lord, W.K., MacMartin, D.G., and Tillman, G., 2000. "Flow Control Opportunities in Gas Turbine Engines". *AIAA 2000-2234*.

[7] NUMECA International, 2007. *FINE^{TM}/Turbo v8, User Manual*. NUMECA International, Brussels.

[8] Spalart, P.R., and Allmaras, S.R., 1992. "A One-Equation Turbulence Model for Aerodynamic Flows". *AIAA 92-0439*.

[9] Greenblatt, D., and Wygnanski, I.J., 2000. "The Control of Flow Separation by Periodic Excitation". *Progress in Aerospace Sciences,* ***36***, pp. 487–545.

[10] Rumsey, C. L., 2007. "Proceedings of the 2004 Workshop on CFD Validation of Synthetic Jets and Turbulent Separation Control". *NASA CP-2007-214874*.

[11] Mertens, D., Thiele, F., Swoboda, M., and Huppertz, A., 2008. "Transition Modeling Effects on the Simulation of a Stator Cascade with Active Flow Control". *ASME GT2008-50697*.

[12] Gmelin, C., Steger, M., Thiele, F., Huppertz, A., and Swoboda, M., 2010. "Unsteady RANS Simulations of a Highly Loaded Low Aspect Ratio Compressor Cascade with Active Flow Control". *ASME GT2010-22516*.

[13] Gmelin, C., Steger, M., Wassen, E., Thiele, F., Huppertz, A., and Swoboda, M., 2010. "URANS Simulations of Active Flow Control on Highly Loaded Turbomachinery Blades". In Active Flow Control II, King, R., ed., Notes on Numerical Fluid Mechanics and Multidisciplinary Design, Springer.

[14] Hecklau, M., Zander, V., Peltzer, I., Nitsche, W., Huppertz, A., and Swoboda, M., 2010. "Experimental AFC Approaches on a Highly Loaded Compressor Cascade". In Active Flow Control II, King, R., ed., Notes on Numerical Fluid Mechanics and Multidisciplinary Design, Springer.

[15] Zander, V., Hecklau, M., Nitsche, W., Huppertz, A., and Swoboda, M., 2009. "Active Control of Corner Vortices on a Highly Loaded Compressor Cascade". *8th European Turbomachinery Conference, Graz*.

[16] Hecklau, M., Zander, V., Nitsche, W., Huppertz, A., and Swoboda, M., 2010. "Active Secondary Flow Control on a Highly Loaded Compressor Cascade by Periodically Pulsating Jets". Dillmann, A., Heller, G., Klaas, M., Kreplin, H.P., Nitsche, W., and Schröder, W., eds., Vol. 108 of *Notes on Numerical Fluid Mechanics and Multidisciplinary Design*, Springer.

[17] Hecklau, M., Zander, V., Nitsche, W., Huppertz, A., and Swoboda, M., 2009. "Time Resolved Particle Image Velocimetry of Active Flow Control on a Compressor Cascade". *8th International Symposium on Particle Image Velocimetry, Melbourne, Australia*.

[18] NUMECA International, 2007. *AutoGrid^{TM} v8, User Manual*. NUMECA International, Brussels.

[19] Weber, A., 2008. *G3DMESH v4.5.4*. DLR, Institut für Antriebstechnik, Köln.

[20] NUMECA International, 2007. *IGG^{TM} v8, User Manual*. NUMECA International, Brussels.

[21] Jameson, A., and Baker, T.J., 1984. "Multigrid Solution of the Euler Equations for Aircraft Configurations". *AIAA Paper 84-00931984*.

[22] Zhu, Z.W., Lacor, C., and Hirsch, C., 1994. "A New Residual Smoothing Method for Multigrid Acceleration Applied to the Navier-Stokes Equations". In Multigrid Methods IV, Hemker, P.W. and Wesseling, P., eds., International Series of Numerical Mathematics, Birkhäuser.

[23] Jameson, A., 1991. "Time Dependent Calculations Using Multigrid with Applications to Unsteady Flows Past Airflois and Wings". *AIAA Paper 91-1596*.

[24] Crowther, W. J., and Gomes, L. T., 2008. "An Evaluation of the Mass and Power Scalling of Synthetic Jet Actuator Flow Control Technology for Civil Transport Aircraft Applications". *Journal of Systems and Control Engineering,* ***222***, pp. 357–372.